# Noncapture transfer in low-energy heavy-ion collisions based on a dinuclear system model

Xingxin Luo,[1] Cheng Li,[1,*] Ya-Xian Wu,[1] Yu-Bing Li,[1] Xin-Rui Zhang,[1,†] Junlong Tian,[1,‡] Qianqian Du,[1,§] Ning Wang,[1,‖] Hui-Xiao Duan,[2] and Feng-Shou Zhang[3,4,5]

[1]*Guangxi Key Laboratory of Nuclear Physics and Technology, Guangxi Normal University, Guilin 541004, China*
[2]*Department of Physics, Changzhi University, Changzhi 046011, China*
[3]*Key Laboratory of Beam Technology of Ministry of Education, School of Physics and Astronomy, Beijing Normal University, Beijing 100875, China*
[4]*Institute of Radiation Technology, Beijing Academy of Science and Technology, Beijing 100875, China*
[5]*Center of Theoretical Nuclear Physics, National Laboratory of Heavy Ion Accelerator of Lanzhou, Lanzhou 730000, China*

(Received 20 January 2026; revised 4 May 2026; accepted 26 May 2026; published 14 July 2026)

We propose an improved dinuclear system (DNS) model to describe both capture and noncapture transfer reactions within a unified framework. The main improvements in this work include the introduction of noncapture transfer processes and dynamic deformation mechanisms. The multinucleon transfer (MNT) reactions of $^{58,64}$Ni + $^{208}$Pb are used to test the improved model. The results show that the improved DNS model can successfully calculate the observables including mass distributions, total kinetic energy–mass distributions, and isotopic cross sections from both capture and noncapture transfer processes. These results indicate that the present DNS model is an effective tool for efficiently calculating product cross sections and investigating energy dissipation mechanisms in MNT reactions.

DOI: 10.1103/sqhm-bpsb

## I. INTRODUCTION

Transfer reaction in low-energy heavy-ion collisions has attracted significant interest in both experimental [1–12] and theoretical [13–36] research. It is widely employed to investigate the key issues in nuclear physics, including nucleon-nucleon interactions [37], the correlation between nuclear reactions and nuclear structure [38], and nuclear spectroscopy [39,40]. When multiple nucleons are transferred between the projectile and the target, this process is termed a multinucleon transfer (MNT) reaction. Currently, the MNT reaction is regarded as a highly promising method for synthesizing new neutron-rich nuclei near $N = 126$ [41–43] and superheavy nuclei close to the predicted "island of stability" by the shell model [44,45].

The nucleon transfer between the reaction partners is governed by multiple degrees of freedom, such as mass asymmetry, deformation, and excitation energy, as well as quantum effects. Hence the transfer reaction is an extremely complex dynamic process. For systems with a pocket in the nucleus-nucleus interaction potential, transfer reactions can be classified into two types based on whether the projectile is captured by the target [46,47]. If the projectile overcomes the Coulomb barrier and is captured by the target, the reaction partners undergo a prolonged nucleon transfer process accompanied by significant energy dissipation, finally separating from each other [48–50]. This type of transfer reaction is referred to as a capture transfer reaction or quasifission (QF) reaction. In contrast, if nucleon transfer occurs without capture, this process is termed a noncapture transfer reaction or scattering process. It includes quasielastic scattering and deep-inelastic scattering. The time scale for noncapture transfer reactions is significantly shorter than those for capture transfer reactions. The capture and noncapture events can be distinguished from the total kinetic energy–mass (TKE-mass) distribution of the primary binary products [51].

The noncapture transfer reactions, primarily deep-inelastic scattering processes, play a crucial role in producing exotic neutron-rich nuclei. In the reactions, numerous combinations of projectilelike fragments (PLFs) and targetlike fragments (TLFs) can be produced. For example, in Ref. [52], deep sub-barrier collisions between $^{40}$Ca and $^{208}$Pb were performed by Cook *et al*. at Legnaro using the PRISMA magnetic spectrometer. They found that reactions of $^{40}$Ca + $^{208}$Pb experience an "explosion" of mass and charge transfers between the nuclei before capture, with unexpectedly high probability. Ninety different combinations of the projectilelike and targetlike nuclei were observed. The noncapture transfer reaction does not result in complete momentum transfer, leading to less energy being dissipated into the system. This characteristic is critical for the survival of primary neutron-rich products.

To calculate the cross sections of products in transfer reactions, several models have been developed, including the improved quantum molecular dynamics (ImQMD) model [27,53,54], the DNS model [33,55–57], the GRAZING model

*Contact author: licheng@mail.bnu.edu.cn
†Contact author: zhangxinrui@gxnu.edu.cn
‡Contact author: tianjl@gxnu.edu.cn
§Contact author: dqianqian@gxnu.edu.cn
‖Contact author: wangning@gxnu.edu.cn

 

[58,59], and the quantal diffusion approach based on stochastic mean-field (SMF) theory [60,61]. The ImQMD model, a microscopic approach, provides a self-consistent description of heavy-ion collisions in both capture and noncapture processes. However, its dynamical simulations are computationally intensive. In contrast, the DNS model offers high computational efficiency for calculating the cross sections of products and describes few-nucleon transfer cross sections very well for heavy systems, such as $^{136}Xe + {}^{198}Pt$ [57] and $^{238}U + {}^{238}U$ [62]. However, it strongly underestimates the cross sections of quasielastic products for light systems due to the absence of contributions from noncapture transfer channels.

To incorporate the cross sections of both capture and noncapture transfer products for light systems, Wen *et al.* developed a hybrid method [63]. They used the GRAZING model to describe noncapture transfer reactions and employed the DNS model to calculate the cross sections of products for capture processes. However, this hybrid method is based on two different theoretical frameworks, which results in a lack of self-consistency. Liao *et al.* introduced impact-parameter-dependent transition probabilities into the DNS-sysu model, providing a unified description of few-nucleon and many-nucleon transfer in MNT reactions. As a result, the cross sections of quasielastic products have been significantly enhanced [64]. In this work, we extend the DNS model by incorporating noncapture transfer mechanisms. This provides a unified framework for calculating the cross sections of all transfer reaction products.

The structure of this paper is as follows. In Sec. II, we describe the theoretical framework in detail. The results and discussion are presented in Sec. III. Finally the conclusion is given in Sec. IV.

## II. THEORETICAL FRAMEWORK

In this work, we developed an improved version of the DNS model by incorporating noncapture transfer mechanisms. The production cross section of the primary fragment with proton number $Z_1$ and neutron number $N_1$ in transfer reactions can be expressed as

$$\sigma_{\rm pr}(Z_1, N_1, E_{\rm c.m.}) = \sigma_1(Z_1, N_1, E_{\rm c.m.}) + \sigma_2(Z_1, N_1, E_{\rm c.m.}). \tag{1}$$

Here, $\sigma_1$ and $\sigma_2$ represent the cross sections of primary fragments produced in the capture and noncapture processes, respectively, given by

$$\sigma_1(Z_1, N_1, E_{\rm c.m.}) = \frac{\pi\hbar^2}{2\mu E_{\rm c.m.}} \sum_J (2J+1) P_{\rm cap}(E_{\rm c.m.}, J) P_1(Z_1, N_1, t=\tau_1), \tag{2}$$

$$\sigma_2(Z_1, N_1, E_{\rm c.m.}) = \frac{\pi\hbar^2}{2\mu E_{\rm c.m.}} \sum_J (2J+1)[1 - P_{\rm cap}(E_{\rm c.m.}, J)] P_2(Z_1, N_1, t=\tau_2). \tag{3}$$

Here, $\mu$ is the reduced mass of the system. $P_{\rm cap}(E_{\rm c.m.}, J)$ represents the capture probability of the projectile. $P_1(Z_1, N_1, t)$ and $P_2(Z_1, N_1, t)$ denote the probability distribution functions for the capture and noncapture processes, respectively. $\tau_1$ and $\tau_2$ are the corresponding interaction times of the colliding nuclei, which are obtained by solving the deflection function [65–67]. For a given angular momentum, the reaction positions for capture and noncapture processes are different, which results in a minor difference between the interaction times $\tau_1$ and $\tau_2$.

The capture probability $P_{\rm cap}(E_{\rm c.m.}, J)$ is written as follows [68,69]:

$$P_{\rm cap}(E_{\rm c.m.}, J) = \begin{cases} 1, & \text{if } E_{\rm c.m.} > V_{\rm B}, \\ \left\{1 + \exp\left\{-\frac{2\pi}{\hbar\omega(J)}[E_{\rm c.m.} - V_{\rm B}(J)]\right\}\right\}^{-1}, & \text{if } V_{\rm b} < E_{\rm c.m.} \leqslant V_{\rm B}, \\ 0, & \text{if } E_{\rm c.m.} \leqslant V_{\rm b}, \end{cases} \tag{4}$$

where $\hbar\omega(J) = \hbar\sqrt{-\frac{1}{\mu}\frac{\partial^2}{\partial r^2}V(R,J)}|_{R=R_{\rm B}(J)}$ is the width of the potential barrier. Figure 1 shows the nucleus-nucleus interaction potentials of $^{48}Ca + {}^{238}U$ with angular momenta $J = 0$ and $125\hbar$. The Coulomb potential and the nuclear potential are calculated with Eqs. (5) and (6), respectively. $V_{\rm B}$ and $V_{\rm b}$ are the Coulomb barrier height and the value of the potential pocket at the bottom, respectively. As shown in Fig. 1, for $J = 0\hbar$, the projectile dissipates its kinetic energy and is captured by the target. In this case, $P_{\rm cap} = 1$, and nucleon transfer occurs at the bottom of the potential pocket. For larger angular momentum (e.g., $J = 125\hbar$), the projectile cannot be captured by the target. Nucleon transfer takes place at an empirical position given by $R_{\rm cont} = R_{\rm close} + 0.8$ fm, where $R_{\rm close}$ satisfies $V(R_{\rm close}, J) = E_{\rm c.m.}$.

The nucleus-nucleus interaction potential is a key quantity for calculating the capture probability. The Coulomb interaction is regarded as follows [70–72]:

$$V_{\rm C}(R) = \begin{cases} \frac{Z_1Z_2e^2}{2R_0}\left(3 - \frac{R^2}{R_0^2}\right), & R < R_0, \\ \frac{Z_1Z_2e^2}{R}, & R \geqslant R_0. \end{cases} \tag{5}$$

Here, $R_0$ denotes the sum of radii of two colliding nuclei. The original DNS model employs the double-folding potential to compute the nuclear interaction. However, this potential

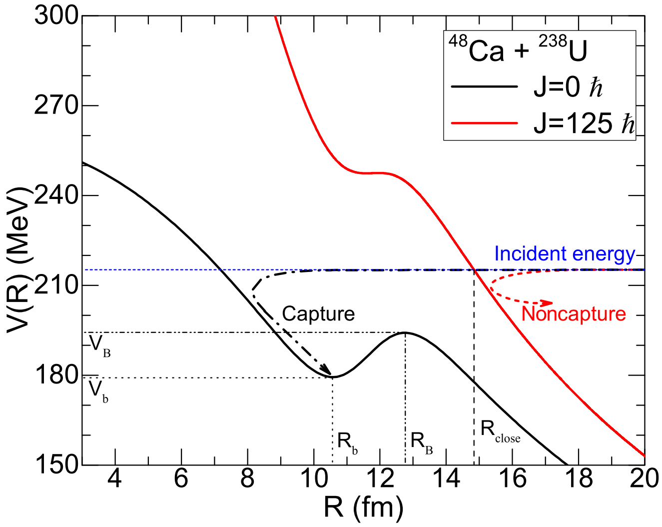


FIG. 1. Nucleus-nucleus interaction potentials of the $^{48}\mathrm{Ca} + {}^{238}\mathrm{U}$ system at $J = 0$ and $125\hbar$. The incident energy is marked by the blue dashed line.

significantly underestimates the barrier height for many reaction systems. As shown in Fig. 2, the dashed lines are the barrier heights extracted from experimental data using the modified Siwek-Wilczyński (MSW) formula [73]. It can be seen that the barrier heights from the double-folding potential are 10–20 MeV lower compared to the results of the MSW formula. In this work, we replace the double-folding

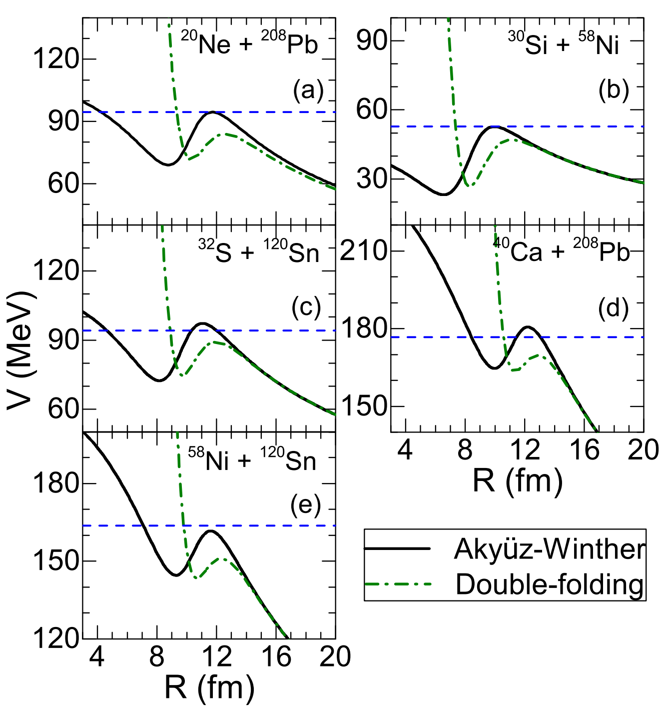


FIG. 2. Nucleus-nucleus interaction potentials for five reaction systems, calculated using the Akyüz-Winther and the double-folding potentials. The dashed lines indicate the barrier heights extracted from experimental data via the MSW formula [73].

potential with the Akyüz-Winther potential [63,74], which can be written as

$$V_{\mathrm{N}}(R) = -16\pi\gamma a \frac{R_1 R_2}{R_1 + R_2} \frac{1}{1 + \exp[(R - R_1 - R_2)/a]}, \quad (6)$$

where

$$\frac{1}{a} = 1.17\left[1 + 0.53\left(A_1^{-1/3} + A_2^{-1/3}\right)\right],$$
$$R_i = 1.2A_i^{1/3} - 0.09,$$
$$\gamma = 0.95\left[1 - 1.8\frac{(N_1 - Z_1)(N_2 - Z_2)}{A_1 A_2}\right]. \quad (7)$$

In the above formula, $A_i$, $Z_i$, and $N_i$ represent the mass number, atomic number, and neutron number of the $i$th nucleus, respectively. One can see that the barrier heights calculated with the Akyüz-Winther potential agree well with the MSW formula.

In the DNS model, solving a set of master equations on the potential energy surface yields the distribution probability of fragments. For a fragment with excitation energy $\varepsilon_1$, proton number $Z_1$, and neutron number $N_1$, its probability distribution function $P(Z_1, N_1, \varepsilon_1, t)$ is predicted by the master equation [43,75,76]:

$$\begin{aligned}\frac{dP(Z_1, N_1, \varepsilon_1, t)}{dt} = &\sum_{Z_1'} W_{Z_1,N_1;Z_1',N_1}(t)\big[d_{Z_1,N_1}P(Z_1', N_1, \varepsilon_1', t) \\ &- d_{Z_1',N_1}P(Z_1, N_1, \varepsilon_1, t)\big] \\ &+ \sum_{N_1'} W_{Z_1,N_1;Z_1,N_1'}(t)\big[d_{Z_1,N_1}P(Z_1, N_1', \varepsilon_1', t) \\ &- d_{Z_1,N_1'}P(Z_1, N_1, \varepsilon_1, t)\big]. \quad (8)\end{aligned}$$

In the above formula, $W_{Z_1,N_1;Z_1,N_1'}$ represents the mean transition probability from the channel $(Z_1, N_1, \varepsilon_1)$ to $(Z_1, N_1', \varepsilon_1')$ [77]. Each transition process focuses on the transfer of a single nucleon, which means that $Z_1' = Z_1 \pm 1$ or $N_1' = N_1 \pm 1$. The quantity $d_{Z_1,N_1'}$ represents the microstate dimension associated with the macrostate $(Z_1, N_1', \varepsilon_1')$. The transition probability can be expressed as [78]

$$\begin{aligned}W_{Z_1,N_1;Z_1,N_1'} = &\frac{\tau_{\mathrm{mem}}(Z_1, N_1; Z_1, N_1')}{\hbar^2 d_{Z_1,N_1} d_{Z_1,N_1'}} \\ &\times \sum_{ii'} |\langle Z_1, N_1', \varepsilon_1', i'|V(t)|Z_1, N_1, \varepsilon_1, i\rangle|^2. \quad (9)\end{aligned}$$

Here, $V(t)$ denotes the single-particle potential obtained from mean-field calculations based on density functional theory [79]. The memory time $\tau_{\mathrm{mem}}$ satisfies $\tau_{\mathrm{mem}} \ll \tau_0/A$; here $\tau_0 \equiv 2\pi\hbar/(1\ \mathrm{MeV}) \approx 40 \times 10^{-22}$ s [77]. In this work, the memory time is set as $\tau_{\mathrm{mem}} = \tau_0/(6A)$ for the capture process and $\tau_{\mathrm{mem}} = \tau_0/(12A)$ for the noncapture process based on a comparison with the experimental data of $^{58,64}\mathrm{Ni} + {}^{208}\mathrm{Pb}$ reactions.

In the DNS model, the nucleon diffusion process is driven by the potential energy surface (PES), which is defined as [80]

$$\begin{aligned} U(Z_1, N_1, \beta_1(t), J(t), R_{\rm cont}) &= \Delta(Z_1, N_1) + \Delta(Z_{\rm tot} - Z_1, N_{\rm tot} - N_1) \\ &+ V_{\rm cont}(Z_1, N_1, \beta_1(t), J(t), R_{\rm cont}) \\ &+ \tfrac{1}{2}C_1(\delta\beta_1)^2 + \tfrac{1}{2}C_2(\delta\beta_2)^2, \end{aligned} \tag{10}$$

where $\Delta(Z_i, N_i)$ is the mass excess of fragments with proton number $Z_i$ and neutron number $N_i$. In the calculation of the mass excess, we employ the temperature-independent pairing correction energy $E_{\rm pair}$ and shell correction energy $E_{\rm shell}$, consistent with Refs. [57,81]. $V_{\rm cont}$ is the interaction potential at the position where nucleon transfer takes place. It includes the Coulomb potential, the nuclear potential, and the centrifugal potential. The Coulomb and nuclear potentials are computed using Eq. (5) and Eq. (6), respectively. The centrifugal potential energy $V_{\rm cent}$ can be expressed as $V_{\rm cent}(R) = J(J+1)\hbar^2/(2\zeta_{\rm rel})$, where $\zeta_{\rm rel}$ denotes the rotational inertia of relative motion in DNS [46]. $R_{\rm cont}$ denotes the interaction radius at the position where nucleon transfer occurs. The dissipation of the relative angular momentum $J(t)$ is described by the following formula [66]:

$$J(t) = J_i \exp(-t/\tau_J) + J_{st}[1 - \exp(-t/\tau_J)], \tag{11}$$

where the limiting value $J_{st}$ given by the sticking condition is $J_{\rm st} = J_i\zeta^0_{\rm rel}/\zeta^0_{\rm tot}$. $\zeta_{\rm rel} = \mu R^2$ ($\zeta^0_{\rm rel} = \mu R_0^2$) and $\zeta^0_{\rm tot} = \mu R_0^2 + \frac{2}{5}m_1R_1^2 + \frac{2}{5}m_2R_2^2$, where $m_1$ and $m_2$ are the masses of the fragments, respectively. $J_i$ denotes the initial angular momentum of system. $\tau_J$ represents the angular momentum relaxation time.

In the nucleon diffusion process, the local excitation energy $\varepsilon_{\rm DNS}$ of the dinuclear system is determined by the dissipation of the kinetic energy of relative motion and the potential energy surface. It is defined as [82,83]

$$\begin{aligned} \varepsilon_{\rm DNS} = E^{\rm diss}(t) - \big[&U(Z_1, N_1, \beta_1(t), \beta_2(t), J(t), R_{\rm cont}) \\ &- U\big(Z_{\rm P}, N_{\rm P}, \beta^0_1, \beta^0_2, J_i, R_{\rm cont}\big)\big], \end{aligned} \tag{12}$$

with

$$\begin{aligned} E^{\rm diss}(t) = E_{\rm c.m.} &- V_{\rm cont}\big(Z_{\rm p}, N_{\rm p}, \beta^0_1, \beta^0_2, J(t), R_{\rm cont}\big) \\ &- E_{\rm rad}(J_i, t). \end{aligned} \tag{13}$$

$\beta^0_1$ and $\beta^0_2$ represent the ground-state deformation of the projectile nucleus and target nucleus, respectively. The radial kinetic energy dissipation can be expressed by solving the Fokker-Planck equation as [55,82]

$$E_{\rm rad}(J_i, t) = E_{\rm rad}(J_i, 0)\exp(-t/\tau_R). \tag{14}$$

Here, $\tau_R$ represents the relaxation time of radial kinetic energy and $E_{\rm rad}(J_i, 0)$ is the radial kinetic energy at the initial moment, which equals $E_{\rm c.m.}$—$V_{\rm cont}(Z_{\rm p}, N_{\rm p}, \beta^0_1, \beta^0_2, J_i, R_{\rm cont})$. The dinuclear system is assumed to quickly reach thermodynamic equilibrium. Therefore, the excitation energy shared by the primary fragments is proportional to their mass, as given by $\varepsilon_i = \varepsilon_{\rm DNS}A_i/A_{\rm tot}$.

During the evolution of the DNS, the colliding nuclei deviate from their ground-state deformations under the Coulomb potential, nuclear potential, and centrifugal potential, leading to a time-dependent PES [84]. We assume that the dynamic deformations of the two nuclei satisfy the relation $\delta\beta_1C_1 = \delta\beta_2C_2$, where the stiffness parameters $C_i$ ($i = 1, 2$) are calculated using the droplet model [85,86]. The mean deformation is defined as $\delta\beta = (\delta\beta_1 + \delta\beta_2)/2$ and is varied from 0 to 1 in steps of 0.01 [64].

The variation of deformation with time can be given by the following formula [87]:

$$\delta\beta(t) = \delta\beta_f(1 - \exp(-t/\tau_\beta)). \tag{15}$$

Here, $\tau_\beta$ represents the deformation relaxation time, while $\delta\beta_f$ indicates the average deformation when two atomic nuclei are in the equilibrium state. The dynamic deformation parameter $\delta\beta_f$ is determined by minimizing the total "intrinsic" energy [87],

$$\begin{aligned} E_{\rm min} = &V_{\rm C}(R, \beta_1, \beta_2) + V_{\rm N}(R, \beta_1, \beta_2) + V_{\rm cent}(R) \\ &+ \sum_{i=1,2}\frac{1}{2}C_i(\delta\beta_i)^2. \end{aligned} \tag{16}$$

Here, $\beta_i = \beta^0_i + \delta\beta_i$. The Coulomb and nuclear potentials including deformation parameters are given by [72]

$$\begin{aligned} V_{\rm C}(R, \beta_1, \beta_2) = \frac{Z_1Z_2e^2}{R}\Bigg\{1 + \frac{1}{R^2}\sum_{i=1,2}R_i^2\Bigg[\sqrt{\frac{9}{20\pi}}\beta_iP_2(\cos\theta_i) \\ + \frac{3}{7\pi}\big(\beta_i^2P_2(\cos\theta_i)\big)^2\Bigg]\Bigg\}, \end{aligned} \tag{17}$$

$$\begin{aligned} V_{\rm N}(R, \beta_1, \beta_2) = -16\pi\gamma a\frac{R_1R_2}{R_1+R_2}\Bigg\{1 + \exp\Bigg\{\Bigg[R - \sum_{i=1,2}R_i \\ \times\left(1 + \sqrt{\frac{5}{4\pi}}\beta_iP_2(\cos\theta_i)\right)\Bigg]\Big/a\Bigg\}\Bigg\}^{-1}. \end{aligned} \tag{18}$$

Here, $\theta_i$ is the orientation angle of the deformed nucleus with respect to the collision axis. In this work, we consider only tip-tip collision orientations. The relaxation times can be determined through the experimental energy spectrum and $\gamma$ multiplicity [66,88]. The values used in our study are as follows: $\tau_R = 3 \times 10^{-22}$ s, $\tau_J = 15 \times 10^{-22}$ s, and $\tau_\beta = 50 \times 10^{-22}$ s [66].

## III. RESULTS AND DISCUSSION

To test the improved DNS model, we first calculated the isotopic cross sections of secondary PLFs in the reactions $^{58}$Ni + $^{208}$Pb at $E_{\rm c.m.} = 269.8$ MeV and $^{64}$Ni + $^{208}$Pb at $E_{\rm c.m.} = 268.0$ MeV. The deexcitation process of the primary fragments is treated with the GEMINI++ code [91,92]. As shown in Fig. 3, the magenta and green lines denote the results for the capture and noncapture processes, respectively. One sees that the cross sections obtained using only capture transfer mechanisms show significant discrepancies from the experimental data in describing the quasielastic peaks of the $0p$ channel for both systems. After incorporating the noncapture transfer mechanism, the quasielastic peaks can be described very well by the improved DNS model

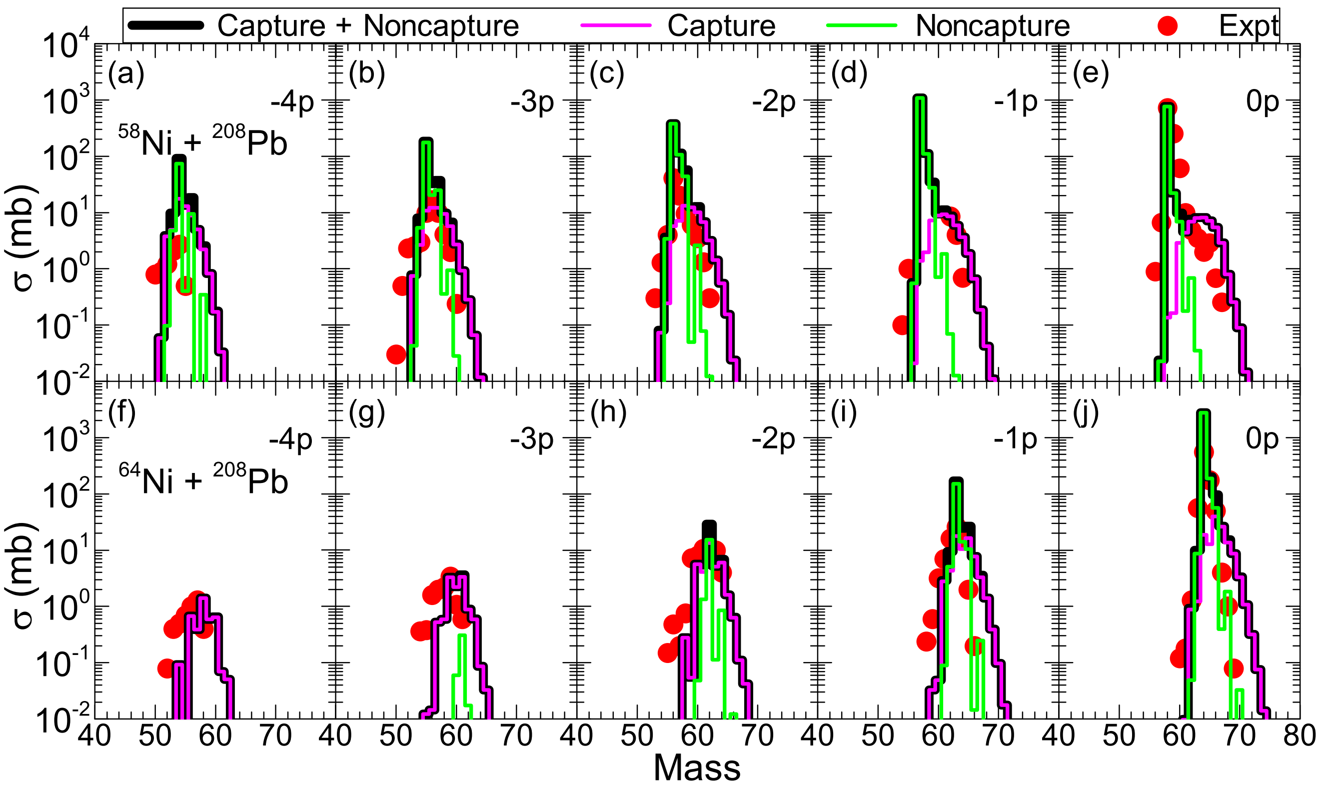


FIG. 3. Isotopic cross sections of secondary PLFs for the reactions $^{58}$Ni + $^{208}$Pb (top panels) at $E_{\mathrm{c.m.}} = 269.8$ MeV and $^{64}$Ni + $^{208}$Pb (bottom panels) at $E_{\mathrm{c.m.}} = 268.0$ MeV. The magenta and green lines denote the results for the capture and noncapture processes, respectively. The black lines represent the total cross sections for th e case of capture + noncapture. The solid circles correspond to the experimental data from Refs. [89,90].

combined with the GEMINI + + code. In addition, we note that, with the increased proton stripping channels, isotopes in the $^{64}$Ni + $^{208}$Pb system are produced primarily through the capture transfer process. The contribution of the noncapture transfer mechanism becomes increasingly small, particularly for the $-3p$ and $-4p$ channels. However, for the $^{58}$Ni + $^{208}$Pb system, the contribution of the noncapture transfer mechanism to the $-1p$ to $-4p$ channels is obviously overestimated, leading to a significant overprediction of the isotopic cross sections compared to the experiment data.

To further test the improved DNS model, Fig. 4 shows the mass distributions of the reactions $^{58}$Ni + $^{208}$Pb and $^{64}$Ni + $^{208}$Pb. The dash-dotted and black lines denote the mass distributions for final fragments from the original and improved DNS models, respectively. It can be seen that the results from the original DNS model significantly deviate from the experimental data near the projectile and target regions. Due to the lack of a noncapture mechanism, the original DNS model underestimates the cross sections of quasielastic peaks by at least one order of magnitude for both the $^{58}$Ni + $^{208}$Pb and $^{64}$Ni + $^{208}$Pb systems. By incorporating the noncapture mechanism, the improved DNS model successfully reproduces the experimental data for both systems. To distinguish the contributions of different mechanisms, we analyzed the mass distributions of final fragments from the capture (magenta lines) and noncapture (green lines) transfer processes within the improved DNS model. One can see

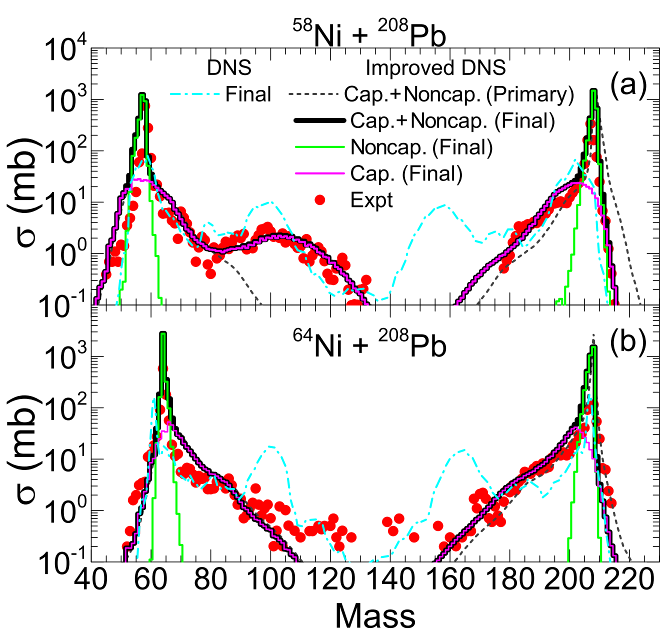


FIG. 4. Mass distributions for the reactions $^{58}$Ni + $^{208}$Pb at $E_{\mathrm{c.m.}} = 269.8$ MeV and $^{64}$Ni + $^{208}$Pb at $E_{\mathrm{c.m.}} = 268.0$ MeV. The dash-dotted lines denote the results of the original DNS model for final fragments. The other lines represent the results of the improved DNS model. The solid circles are experimental data from Refs. [89,90].

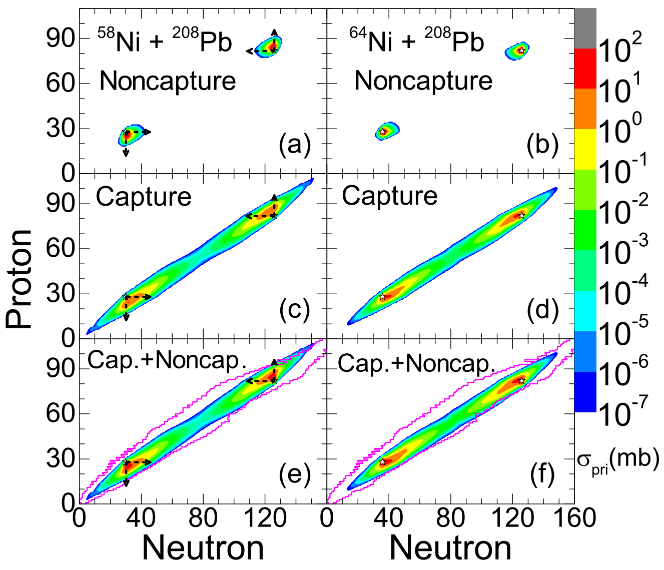


FIG. 5. Calculated production cross sections of primary fragments for the reactions $^{58}$Ni + $^{208}$Pb and $^{64}$Ni + $^{208}$Pb. The top, middle, and bottom panels correspond to the noncapture, capture, and capture + noncapture cases. The stars denote the positions of the projectiles and targets. The arrows indicate the directions of the proton stripping and neutron pickup channels. The folding lines are the boundary of the known nuclei. Cross sections are shown in logarithmic scale in the units of millibarn.

that the fragments produced via the transfer of only a few nucleons are dominated by noncapture mechanisms, whereas fragments with the transfer of more nucleons are produced primarily through capture processes. In addition, we note that, for the $^{58}$Ni + $^{208}$Pb system, the fission fragment distribution in the mass range $80 < A < 130$ is well reproduced by the improved DNS model combined with the GEMINI + + code. Figure 5 shows the two-dimensional cross section distributions of primary fragments for the reactions $^{58}$Ni + $^{208}$Pb and $^{64}$Ni + $^{208}$Pb. From Figs. 5(a) and 5(b), one sees that the noncapture case provides quite narrow distributions in both systems. Only a few nucleons are transferred in noncapture transfer process due to the shorter interaction time between the reaction partners. Furthermore, as these collisions happen in the peripheral region, they result in larger cross sections for products near the projectile and target nuclei. In addition, we note that the enhanced proton stripping and neutron pickup effects can be clearly seen in the neutron-deficient system $^{58}$Ni + $^{208}$Pb. This phenomenon can also be observed in the calculations of the ImQMD model [93]. Figures 5(c) and 5(d) present the cross section distributions for the capture transfer process. It can be seen that the products have broader distributions in both systems due to longer interaction time. A large number of primary fragments can be produced in this process. Figures 5(e) and 5(f) present the distributions for the capture + noncapture case. The distributions of the $^{58}$Ni + $^{208}$Pb and $^{64}$Ni + $^{208}$Pb systems are in good agreement with the results of the SMF model [60].

In MNT reactions, the different reaction mechanisms can be distinguished from the TKE-mass distribution of the primary products [94]. The total kinetic energy (TKE) of the PLF and TLF at the exit channel is given by TKE $\approx E_{c.m.} + Q_{gg} - \varepsilon_{DNS}$, where $E_{c.m.}$, $Q_{gg}$, and $\varepsilon_{DNS}$ are the incident energy, the reaction $Q$ value under the ground state, and the local excitation energy of primary binary fragments, respectively. Figure 6 shows the calculated TKE-mass distributions for the $^{58}$Ni + $^{208}$Pb system at $E_{c.m.} = 269.8$ MeV. The fusion-fission events are not included. From Fig. 6(a), it can be seen that the original DNS model cannot describe the distributions of quasielastic events due to the lack of an effective noncapture transfer mechanism. In addition, the TKE of the intermediate mass fragments is significantly greater than that predicted by the Viola systematics [95]. With the inclusion of noncapture transfer and dynamic deformation mechanisms to the original DNS model, it can be observed in Fig. 6(b) that the TKE-mass distribution from the improved DNS model exhibits clear quasielastic and deep-inelastic collision features. This distribution is highly similar to the results of the ImQMD model [see Fig. 6(e)] and the experimental data for the $^{48}$Ca + $^{232}$Th and $^{48}$Ca + $^{238}$U systems [96]. The distributions for the noncapture and capture transfer processes are shown in Figs. 6(c) and 6(d), respectively. One can see that the distribution of the capture process exhibits typical QF features and is largely consistent with the Viola systematics, while the noncapture case shows a distribution characteristic of deep-inelastic collisions. For comparison, the TKE-mass distributions for noncapture ($0 < t_{con} \leqslant 400$ fm/c) and capture ($400 < t_{con} \leqslant 1000$ fm/c) events, as calculated by the ImQMD model, are shown in Figs. 6(f) and 6(g), respectively.

## IV. CONCLUSIONS

In this article, an improved version of the DNS model is developed to describe MNT reactions in both the capture and noncapture transfer processes within a unified framework. The noncapture transfer mechanisms have been introduced to describe nucleon transfer processes in quasielastic and deep-inelastic collisions. In addition, we have optimized the calculations of the potential energy surface by introducing dynamic deformation and adopted a modified memory time parameter. The mass distributions, TKE-mass distributions, and isotopic cross sections in MNT reactions of $^{58}$Ni + $^{208}$Pb and $^{64}$Ni + $^{208}$Pb are calculated by the improved DNS model. The results show that (1) the quasielastic peaks of the mass distributions of these two systems can be reproduced very well compared with original DNS model, (2) the TKE-mass distribution from the improved DNS model exhibits clear quasielastic and deep-inelastic collision features and is highly similar to the results of the ImQMD model, and (3) the two-dimensional cross section distributions of primary fragments for the $^{58,64}$Ni + $^{208}$Pb reactions are in good agreement with those from the SMF model. However, for the $^{58}$Ni + $^{208}$Pb system, the improved DNS model overpredicts the noncapture transfer cross sections in larger proton stripping channels. We will further improve our model in the next work.

## ACKNOWLEDGMENTS

We acknowledge computing support by the High Performance Computing Platform at Guangxi Key Laboratory of

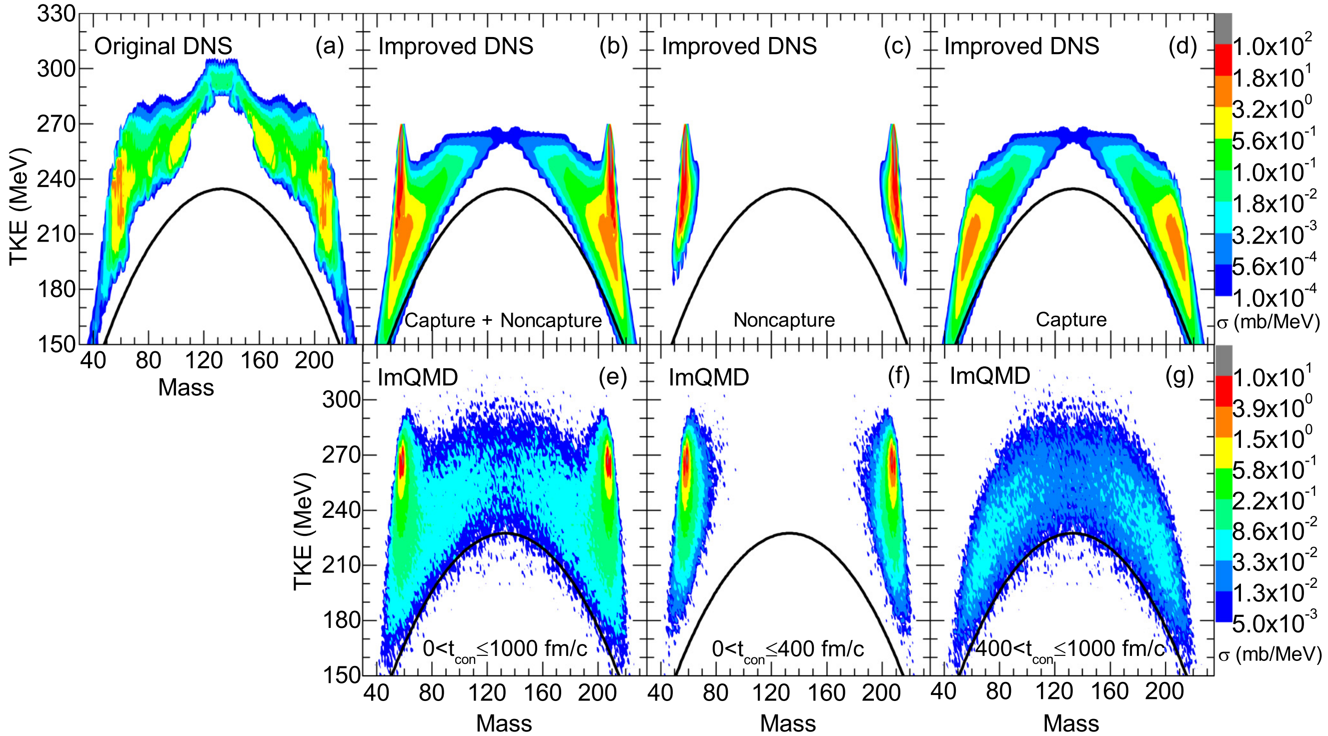


FIG. 6. Calculated TKE-mass distributions of the primary binary fragments for the reaction $^{58}$Ni + $^{208}$Pb at $E_{c.m.} = 269.8$ MeV. Panel (a) shows the results from the original DNS model, while panels (b), (c), and (d) show those from the improved DNS model for the cases of capture + noncapture, noncapture, and capture, respectively. The bottom panels are the results from the ImQMD model in different contact time ranges. The solid lines represent the TKE of the products as predicted by the Viola systematics. The contour plots are the differential cross sections (in units of [mb/MeV]) in logarithmic scale.

Nuclear Physics and Technology. This work was supported by the Guangxi Natural Science Foundation under Grants No. 2023GXNSFBA026027, No. 2023GXNSFBA026008, No. 2023GXNSFDA026005, and No. 2024GXNSFBA010377, the National Natural Science Foundation of China under Grants No. 12465021, No. 12465019, No. 12135004, No. 11635003, and No. 11961141004, the National Key R&D Program of China under Grant No. 2023YFA1606401, the Basic research program of Shanxi Province (Grant No. 202203021212171), the Guangxi "Bagui Scholar" Teams for Innovation and Research Project, the Central Government Guidance Funds for Local Scientific and Technological Development, China (Grant No. Guike ZY22096024), and the Guangxi Normal University National Natural Science Foundation joint cultivation project (No. 2025PY010).

## DATA AVAILABILITY

The data that support the findings of this article are openly available [89,90].


[1] L. Corradi, G. Pollarolo, and S. Szilner, Multinucleon transfer processes in heavy-ion reactions, J. Phys. G: Nucl. Part. Phys. **36**, 113101 (2009).

[2] S. B. Ma, L. N. Sheng, X. H. Zhang, S. T. Wang, K. L. Wang, C. W. Ma, H. J. Ong, Z. Y. Sun, S. W. Tang, Y. H. Yu, X. T. Du, and X. B. Wei, Opportunities for production and property research of neutron-rich nuclei around $N = 126$ at HIAF, Nucl. Sci. Tech. **35**, 97 (2024).

[3] E. M. Kozulin, G. N. Knyazheva, A. V. Karpov, V. V. Saiko, A. A. Bogachev, I. M. Itkis, K. V. Novikov, I. V. Vorobiev, I. V. Pchelintsev, E. O. Savelieva, R. S. Tikhomirov, M. G. Itkis, and Y. T. Oganessian, Detailed study of multinucleon transfer features in the $^{136}$Xe + $^{238}$U reaction, Phys. Rev. C **109**, 034616 (2024).

[4] S. Koulouris, G. A. Souliotis, F. Cappuzzello, D. Carbone, A. Pakou, C. Agodi, G. A. Brischetto, S. Calabrese, M. Cavallaro, I. Ciraldo, O. Fasoula, J. Klimo, O. Sgouros, V. Soukeras, A. Spatafora, D. Torresi, and M. Veselsky, Multinucleon transfer channels from $^{70}$Zn (15 MeV/nucleon) + $^{64}$Ni collisions, Phys. Rev. C **108**, 044612 (2023).

[5] T. Niwase, Y. X. Watanabe, Y. Hirayama, M. Mukai, P. Schury, A. N. Andreyev, T. Hashimoto, S. Iimura, H. Ishiyama, Y. Ito, S. C. Jeong, D. Kaji, S. Kimura, H. Miyatake, K. Morimoto, J. Y. Moon, M. Oyaizu, M. Rosenbusch, A. Taniguchi, and M. Wada, Discovery of new isotope $^{241}$U and systematic high-precision atomic mass measurements of neutron-rich Pa-Pu nuclei produced via multinucleon transfer reactions, Phys. Rev. Lett. **130**, 132502 (2023).

[6] J. Diklić, S. Szilner, L. Corradi, T. Mijatović, G. Pollarolo, P. Čolović, G. Colucci, E. Fioretto, F. Galtarossa, A. Goasduff, A. Gottardo, J. Grebosz, A. Illana, G. Jaworski, M. J. Gomez, T. Marchi, D. Mengoni, G. Montagnoli, D. Nurkić, M. Siciliano, *et al.*, Transfer reactions in $^{206}$Pb + $^{118}$Sn: From quasielastic to deep-inelastic processes, Phys. Rev. C **107**, 014619 (2023).

[7] R. M. P. Vidal, F. Galtarossa, T. Mijatović, S. Szilner, I. Zanon, D. Brugnara, J. Pellumaj, M. Ciemala, J. J. V. Dobón, L. Corradi, E. Clément, S. Leoni, B. Fornal, M. Siciliano, and A. Gadea, Nuclear structure advancements with multi-nucleon transfer reactions, Eur. Phys. J. A **59**, 114 (2023).

[8] S. Heinz and H. M. Devaraja, Nucleosynthesis in multinucleon transfer reactions, Eur. Phys. J. A **58**, 114 (2022).

[9] V. V. Desai, W. Loveland, R. Yanez, G. Lane, S. Zhu, A. D. Ayangekaa, J. P. Greene, F. G. Kondev, R. V. F. Janssens, and P. A. Copp, The $^{136}$Xe + $^{198}$Pt reaction: A detailed reexamination, Eur. Phys. J. A **56**, 150 (2020).

[10] T. Welsh, W. Loveland, R. Yanez, J. S. Barrett, E. A. McCutchan, A. A. Sonzogni, T. Johnson, S. Zhu, J. P. Greene, A. D. Ayangeakaa, M. P. Carpenter, T. Lauritsen, J. L. Harker, W. B. Walters, B. M. S. Amro, and P. Copp, Modeling multinucleon transfer in symmetric collisions of massive nuclei, Phys. Lett. B **771**, 119 (2017).

[11] Y. X. Watanabe, Y. H. Kim, S. C. Jeong, Y. Hirayama, N. Imai, H. Ishiyama, H. S. Jung, H. Miyatake, S. Choi, J. S. Song, E. Clement, G. de France, A. Navin, M. Rejmund, C. Schmitt, G. Pollarolo, L. Corradi, E. Fioretto, D. Montanari, M. Niikura, *et al.*, Pathway for the production of neutron-rich isotopes around the $N = 126$ shell closure, Phys. Rev. Lett. **115**, 172503 (2015).

[12] J. S. Barrett, W. Loveland, R. Yanez, S. Zhu, A. D. Ayangeakaa, M. P. Carpenter, J. P. Greene, R. V. F. Janssens, T. Lauritsen, E. A. McCutchan, A. A. Sonzogni, C. J. Chiara, J. L. Harker, and W. B. Walters, $^{136}$Xe + $^{208}$Pb reaction: A test of models of multinucleon transfer reactions, Phys. Rev. C **91**, 064615 (2015).

[13] V. Zagrebaev and W. Greiner, Production of new heavy isotopes in low-energy multinucleon transfer reactions, Phys. Rev. Lett. **101**, 122701 (2008).

[14] Z. H. Wang, Y. L. Zhang, and Z. Q. Feng, Dynamics of light nuclei produced in the massive transfer reactions, Nucl. Sci. Tech. **36**, 229 (2025).

[15] N. Tang, S. Y. Ma, R. An, J. J. Li, and F. S. Zhang, Production of unknown neutron-deficient isotopes with $Z = 99$–106 in multinucleon transfer reaction $^{124}$Xe + $^{249}$Cf, Nucl. Sci. Tech. **36**, 44 (2025).

[16] Y. Zou, M. H. Zhang, M. C. Wang, Y. H. Zhang, and F. S. Zhang, Investigation of multinucleon transfer processes in the Langevin equation model, Nucl. Sci. Tech. **35**, 180 (2024).

[17] L. Zhu, New model based on coupling the master and Langevin equations in the study of multinucleon transfer reactions, Phys. Lett. B **849**, 138423 (2024).

[18] Y. H. Zhang, J. J. Li, C. Li, M. H. Zhang, Y. Zou, and F. S. Zhang, Microscopic study of the production of neutron-rich isotopes near $N = 126$ in the multinucleon transfer reactions $^{78,82,86}$Kr + $^{208}$Pb, Phys. Rev. C **109**, 044617 (2024).

[19] H. Yao, C. Li, H. B. Zhou, and N. Wang, Distinguishing fission-like events from deep-inelastic collisions, Phys. Rev. C **109**, 034608 (2024).

[20] Z. H. Liao, Z. P. Gao, Y. Yang, L. Zhu, and J. Su, Shell effects on the drift and fluctuation in multinucleon transfer reactions, Phys. Rev. C **109**, 054612 (2024).

[21] Z. Q. Feng, Effect of cluster transfer on the production of neutron-rich nuclides near $N = 126$ in multinucleon-transfer reactions, Phys. Rev. C **108**, L051601 (2023).

[22] M. Arik, S. Ayik, O. Yilmaz, and A. S. Umar, Description of the multinucleon transfer mechanism for $^{48}$Ca + $^{244}$Pu and $^{86}$Kr + $^{198}$Pt reactions in a quantal transport approach, Phys. Rev. C **108**, 064604 (2023).

[23] P. H. Chen, C. Geng, Z. X. Yang, X. H. Zeng, and Z. Q. Feng, Production of neutron-rich actinide isotopes in isobaric collisions via multinucleon transfer reactions, Nucl. Sci. Tech. **34**, 160 (2023).

[24] S. Ayik, M. Arik, E. Erbayri, O. Yilmaz, and A. S. Umar, Multinucleon transfer mechanism in $^{160}$Gd + $^{186}$W collisions in stochastic mean-field theory, Phys. Rev. C **108**, 054605 (2023).

[25] X. J. Bao, Optimal condition for the production of heavy and superheavy neutron-rich isotopes with multinucleon transfer reaction, Phys. Lett. B **833**, 137307 (2022).

[26] B. J. Roy, S. Santra, A. Pal, H. Kumawat, S. K. Pandit, V. V. Parkar, K. Ramachandran, K. Mahata, and K. Sekizawa, Reaction mechanism study for multinucleon transfer processes in collisions of spherical and deformed nuclei at energies near and above the Coulomb barrier: The $^{16}$O + $^{154}$Sm reaction, Phys. Rev. C **105**, 044611 (2022).

[27] K. Zhao, Z. Liu, F. S. Zhang, and N. Wang, Production of neutron-rich $N = 126$ nuclei in multinucleon transfer reactions: Comparison between $^{136}$Xe + $^{198}$Pt and $^{238}$U + $^{198}$Pt reactions, Phys. Lett. B **815**, 136101 (2021).

[28] L. Zhu, C. Li, C. C. Guo, J. Su, P. W. Wen, G. Zhang, and F. S. Zhang, Theoretical progress on production of isotopes in the multinucleon transfer process, Int. J. Mod. Phys. E **29**, 2030004 (2020).

[29] S. A. Kalandarov, G. G. Adamian, N. V. Antonenko, H. M. Devaraja, and S. Heinz, Production of neutron deficient isotopes in the multinucleon transfer reaction $^{48}$Ca ($E_{\rm lab} = 5.63$ MeV/nucleon) + $^{248}$Cm, Phys. Rev. C **102**, 024612 (2020).

[30] G. G. Adamian, N. V. Antonenko, A. D. Torres, and S. Heinz, How to extend the chart of nuclides? Eur. Phys. J. A **56**, 47 (2020).

[31] X. Jiang and N. Wang, Probing the production mechanism of neutron-rich nuclei in multinucleon transfer reactions, Phys. Rev. C **101**, 014604 (2020).

[32] G. Zhang, C. A. T. Sokhna, Z. Liu, and F. S. Zhang, Production of neutron-rich isotopes $^{264,266,268,269}$Rf by multinucleon transfer reactions based on $^{238}$U beam, Phys. Rev. C **100**, 024613 (2019).

[33] S. Q. Guo, X. J. Bao, H. F. Zhang, J. Q. Li, and N. Wang, Effect of dynamical deformation on the production distribution in multinucleon transfer reactions, Phys. Rev. C **100**, 054616 (2019).

[34] M. H. Mun, K. Kwak, G. G. Adamian, and N. V. Antonenko, Possible production of neutron-rich Md isotopes in multinucleon transfer reactions with Cf and Es targets, Phys. Rev. C **99**, 054627 (2019).

[35] F. S. Zhang, C. Li, L. Zhu, and P. W. Wen, Production cross sections for exotic nuclei with multinucleon transfer reactions, Front. Phys. **13**, 132113 (2018).

[36] N. Wang and L. Guo, New neutron-rich isotope production in $^{154}$Sm + $^{160}$Gd, Phys. Lett. B **760**, 236 (2016).
[37] J. L. Ferreira, J. Lubian, F. Cappuzzello, M. Cavallaro, and D. Carbone, Multinucleon transfer in the $^{116}$Cd ($^{20}$Ne, $^{20}$O) $^{116}$Sn double charge exchange reaction at 306 MeV incident energy, Phys. Rev. C **105**, 014630 (2022).
[38] S. Szilner, C. A. Ur, L. Corradi, N. Mărginean, G. Pollarolo, A. M. Stefanini, S. Beghini, B. R. Behera, E. Fioretto, A. Gadea, B. Guiot, A. Latina, P. Mason, G. Montagnoli, F. Scarlassara, M. Trotta, G. de Angelis, F. Della Vedova, E. Farnea, F. Haas, *et al.*, Multinucleon transfer reactions in closed-shell nuclei, Phys. Rev. C **76**, 024604 (2007).
[39] D. Bucurescu, C. Rusu, N. Mărginean, C. A. Ur, G. de Angelis, L. Corradi, D. Bazzacco, S. Beghini, F. Della Vedova, G. Duchene, E. Farnea, T. Faul, E. Fioretto, A. Gadea, W. Gelletly, B. Guiot, M. Ionescu Bujor, A. Iordăchescu, S. D. Landown, S. M. Lenzi, *et al.*, $\gamma$-ray spectroscopy of the neutron-rich nuclei $^{89}$Rb, $^{92}$Y, and $^{93}$Y with multinucleon transfer reactions, Phys. Rev. C **76**, 064301 (2007).
[40] B. Birkenbach, A. Vogt, K. Geibel, F. Recchia, P. Reiter, J. J. V. Dobón, D. Bazzacco, M. Bowry, A. Bracco, B. Bruyneel, L. Corradi, F. C. L. Crespi, G. de Angelis, P. Désesquelles, J. Eberth, E. Farnea, E. Fioretto, A. Gadea, A. Gengelbach, A. Giaz, *et al.*, Spectroscopy of the neutron-rich actinide nucleus $^{240}$U following multinucleon-transfer reactions, Phys. Rev. C **92**, 044319 (2015).
[41] F. C. Dai, P. W. Wen, C. J. Lin, J. J. Liu, X. X. Xu, K. L. Wang, H. M. Jia, L. Yang, and N. R. Ma, Investigation into the production of neutron-rich nuclides in the $N = 126$ region through multinucleon transfer reactions, Phys. Rev. C **112**, 014621 (2025).
[42] Z. H. Liao, L. Zhu, Z. P. Gao, J. Su, and C. Li, Optimal detection angles for producing $N = 126$ neutron-rich isotones in multinucleon transfer reactions, Phys. Rev. Res. **5**, L022021 (2023).
[43] L. Zhu, J. Su, W. J. Xie, and F. S. Zhang, Theoretical study on production of heavy neutron-rich isotopes around the $N = 126$ shell closure in radioactive beam induced transfer reactions, Phys. Lett. B **767**, 437 (2017).
[44] A. Sobiczewski, F. A. Gareev, and B. N. Kalinkin, Closed shells for $Z > 82$ and $N > 126$ in a diffuse potential well, Phys. Lett. **22**, 500 (1966).
[45] M. G. Mayer, On closed shells in nuclei. II, Phys. Rev. **75**, 1969 (1949).
[46] A. Nasirov, A. Fukushima, Y. Toyoshima, Y. Aritomo, A. Muminov, S. Kalandarov, and R. Utamuratov, The role of orientation of nucleus symmetry axis in fusion dynamics, Nucl. Phys. A **759**, 342 (2005).
[47] A. K. Nasirov, A. R. Yusupov, and B. M. Kayumov, Small cross section of the synthesis of darmstadtium in the $^{48}$Ca + $^{232}$Th reaction, Phys. Rev. C **110**, 014618 (2024).
[48] A. K. Nasirov, B. M. Kayumov, G. Mandaglio, G. Giardina, K. Kim, and Y. Kim, The effect of the neutron and proton numbers ratio in colliding nuclei on the formation of the evaporation residues in the $^{34}$S + $^{208}$Pb and $^{36}$S + $^{206}$Pb reactions, Eur. Phys. J. A **55**, 29 (2019).
[49] N. Wang, L. Ou, Y. X. Zhang, and Z. X. Li, Microscopic dynamics simulations of heavy-ion fusion reactions induced by neutron-rich nuclei, Phys. Rev. C **89**, 064601 (2014).
[50] C. Simenel and A. S. Umar, Heavy-ion collisions and fission dynamics with the time-dependent Hartree–Fock theory and its extensions, Prog. Part. Nucl. Phys. **103**, 19 (2018).
[51] E. M. Kozulin, G. N. Knyazheva, I. M. Itkis, M. G. Itkis, A. A. Bogachev, L. Krupa, T. A. Loktev, S. V. Smirnov, V. I. Zagrebaev, J. Äystö, W. H. Trzaska, V. A. Rubchenya, E. Vardaci, A. M. Stefanini, M. Cinausero, L. Corradi, E. Fioretto, P. Mason, G. F. Prete, R. Silvestri, *et al.*, Investigation of the reaction $^{64}$Ni + $^{238}$U being an option of synthesizing element 120, Phys. Lett. B **686**, 227 (2010).
[52] K. J. Cook, D. C. Rafferty, D. J. Hinde, E. C. Simpson, M. Dasgupta, L. Corradi, M. Evers, E. Fioretto, D. Jeung, N. Lobanov, D. H. Luong, T. Mijatović, G. Montagnoli, A. M. Stefanini, and S. Szilner, Colliding heavy nuclei take multiple identities on the path to fusion, Nat. Commun. **14**, 7988 (2023).
[53] C. Li, X. X. Xu, J. J. Li, G. Zhang, B. Li, C. A. T. Sokhna, Z. S. Ge, F. Zhang, P. W. Wen, and F. S. Zhang, Production of new neutron-rich heavy nuclei with $Z = 56–80$ in the multinucleon transfer reactions of $^{136}$Xe + $^{198}$Pt, Phys. Rev. C **99**, 024602 (2019).
[54] K. Zhao, Z. Liu, F. S. Zhang, N. Wang, and J. Z. Duan, Distinct sequential and massive transfer processes for production of neutron-rich $N \approx 126$ nuclei in $^{238}$U + $^{198}$Pt reactions, Phys. Rev. C **106**, L011602 (2022).
[55] Z. Q. Feng, Production of neutron-rich isotopes around $N = 126$ in multinucleon transfer reactions, Phys. Rev. C **95**, 024615 (2017).
[56] X. J. Bao, S. Q. Guo, J. Q. Li, and H. F. Zhang, Influence of neutron excess of projectile on multinucleon transfer reactions, Phys. Lett. B **785**, 221 (2018).
[57] L. Zhu, P. W. Wen, C. J. Lin, X. J. Bao, J. Su, C. Li, and C. C. Guo, Shell effects in a multinucleon transfer process, Phys. Rev. C **97**, 044614 (2018).
[58] A. Winther, Grazing reactions in collisions between heavy nuclei, Nucl. Phys. A **572**, 191 (1994).
[59] A. Winther, Dissipation, polarization and fluctuation in grazing heavy-ion collisions and the boundary to the chaotic regime, Nucl. Phys. A **594**, 203 (1995).
[60] K. Sekizawa and S. Ayik, Quantal diffusion approach for multinucleon transfer processes in the $^{58,64}$Ni + $^{208}$Pb reactions: Toward the production of unknown neutron-rich nuclei, Phys. Rev. C **102**, 014620 (2020).
[61] S. Ayik, A stochastic mean-field approach for nuclear dynamics, Phys. Lett. B **658**, 174 (2008).
[62] L. Zhu, Selection of projectiles for producing trans-uranium nuclei in transfer reactions within the improved dinuclear system model, J. Phys. G: Nucl. Part. Phys. **47**, 065107 (2020).
[63] P. W. Wen, C. Li, L. Zhu, C. J. Lin, and F. S. Zhang, Mechanism of multinucleon transfer reaction based on the GRAZING model and DNS model, J. Phys. G: Nucl. Part. Phys. **44**, 115101 (2017).
[64] Z. H. Liao, Y. Yang, Z. P. Gao, J. Su, and L. Zhu, Mechanism of the quasielastic scattering based on the dinuclear system concept, Phys. Rev. C **112**, L051601 (2025).
[65] X. J. Bao, Possibilities for synthesis of new neutron-deficient isotopes of superheavy nuclei, Chin. Phys. C **43**, 054105 (2019).
[66] C. Riedel, G. Wolschin, and W. Norenberg, Relaxation times in dissipative heavy-ion collisions, Z. Phys. A **290**, 47 (1979).

[67] J. Q. Li and G. Wolschin, Distribution of the dissipated angular momentum in heavy-ion collisions, Phys. Rev. C **27**, 590 (1983).
[68] D. L. Hill and J. A. Wheeler, Nuclear constitution and the interpretation of fission phenomena, Phys. Rev. **89**, 1102 (1953).
[69] B. M. Kayumov, O. K. Ganiev, A. K. Nasirov, and G. A. Yuldasheva, Analysis of the fusion mechanism in the synthesis of superheavy element 119 via the $^{54}$Cr + $^{243}$Am reaction, Phys. Rev. C **105**, 014618 (2022).
[70] D. M. Brink and N. Takigawa, Barrier penetration effects in the semi-classical theory of elastic scattering between complex nuclei, Nucl. Phys. A **279**, 159 (1977).
[71] R. Anni and L. Renna, Semi-classical angular decomposition of the heavy-ion scattering amplitude. contributions from reflected, refracted and diffracted trajectories, Nuov. Cim. A **65**, 311 (1981).
[72] C. J. Lin, J. C. Xu, H. Q. Zhang, Z. H. Liu, F. Yang, and L. X. Lu, Threshold anomaly in the $^{19}$F + $^{208}$Pb system, Phys. Rev. C **63**, 064606 (2001).
[73] Y. R. X. Chen, H. Yao, M. Liu, J. L. Tian, P. W. Wen, and N. Wang, Systematic study of fusion barriers with energy dependent barrier radius, At. Data Nucl. Data Tables **154**, 101587 (2023).
[74] *Nuclear Structure and Heavy-ion Collisions: Varenna on Lake Como, Villa Monastero, 9th–21st July 1979*, edited by R. A. Broglia, R. A. Ricci, C. H. Dasso, and S. I. D. Fisica (North-Holland, Amsterdam, 1981).
[75] L. Zhu, Z. Q. Feng, and F. S. Zhang, Production of heavy neutron-rich nuclei in transfer reactions within the dinuclear system model, J. Phys. G: Nucl. Part. Phys. **42**, 085102 (2015).
[76] L. Zhu, F. S. Zhang, P. W. Wen, J. Su, and W. J. Xie, Production of neutron-rich nuclei with $Z = 60$–73 in reactions induced by Xe isotopes, Phys. Rev. C **96**, 024606 (2017).
[77] W. Nörenberg, Quantum-statistical approach to gross properties of peripheral collisions between heavy nuclei, Z. Phys. A **274**, 241 (1975).
[78] S. Ayik, B. Schürmann, and W. Nörenberg, Microscopic transport theory of heavy-ion collisions, Z. Phys. A **277**, 299 (1976).
[79] P. W. Wen, A. K. Nasirov, C. J. Lin, and H. M. Jia, Multinucleon transfer reaction from view point of dynamical dinuclear system method, J. Phys. G: Nucl. Part. Phys. **47**, 075106 (2020).
[80] G. G. Adamian, N. V. Antonenko, W. Scheid, and V. V. Volkov, Fusion cross sections for superheavy nuclei in the dinuclear system concept, Nucl. Phys. A **633**, 409 (1998).
[81] P. Möller, A. J. Sierk, T. Ichikawa, and H. Sagawa, Nuclear ground-state masses and deformations: FRDM(2012), At. Data Nucl. Data Tables **109–110**, 1 (2016).
[82] Z. Q. Feng, G. M. Jin, F. Fu, and J. Q. Li, Production cross sections of superheavy nuclei based on dinuclear system model, Nucl. Phys. A **771**, 50 (2006).
[83] Z. Q. Feng, G. M. Jin, J. Q. Li, and W. Scheid, Formation of superheavy nuclei in cold fusion reactions, Phys. Rev. C **76**, 044606 (2007).
[84] G. Wolschin, Shape relaxation in heavy-ion collisions, Phys. Lett. B **88**, 35 (1979).
[85] L. Zhu, J. Su, P. W. Wen, C. C. Guo, and C. Li, Multinucleon transfer process in the reaction $^{160}$Gd + $^{186}$W, Phys. Rev. C **98**, 034609 (2018).
[86] W. D. Myers and W. J. Swiatecki, Nuclear masses and deformations, Nucl. Phys. **81**, 1 (1966).
[87] N. Wang, E. G. Zhao, W. Scheid, and S. G. Zhou, Theoretical study of the synthesis of superheavy nuclei with $Z = 119$ and 120 in heavy-ion reactions with trans-uranium targets, Phys. Rev. C **85**, 041601(R) (2012).
[88] G. Wolschin and G. Wolschin, Analysis of relaxation phenomena in heavy-ion collisions, Z. Phys. A **284**, 209 (1978).
[89] W. Królas, R. Broda, B. Fornal, T. Pawłat, H. Grawe, K. H. Maier, M. Schramm, and R. Schubart, Gamma coincidence study of $^{208}$Pb + 350 MeV $^{64}$Ni collisions, Nucl. Phys. A **724**, 289 (2003).
[90] W. Królas, R. Broda, B. Fornal, T. Pawłat, J. Wrzesiński, D. Bazzacco, G. de Angelis, S. Lunardi, R. Menegazzo, D. R. Napoli, and C. Rossi Alvarez, Dynamical deformation of nuclei in deep-inelastic collisions: A gamma coincidence study of $^{130}$Te +275 MeV| $^{64}$Ni and $^{208}$Pb +345 MeV $^{58}$Ni heavy ion reactions, Nucl. Phys. A **832**, 170 (2010).
[91] R. J. Charity, Systematic description of evaporation spectra for light and heavy compound nuclei, Phys. Rev. C **82**, 014610 (2010).
[92] D. Mancusi, R. J. Charity, and J. Cugnon, Unified description of fission in fusion and spallation reactions, Phys. Rev. C **82**, 044610 (2010).
[93] C. Li, T. Li, X. R. Zhang, J. L. Tian, N. Wang, C. C. Guo, and F. S. Zhang, Inverse transfer mechanisms in multinucleon transfer reactions, Phys. Rev. C **110**, 044615 (2024).
[94] C. Li, J. L. Tian, and F. S. Zhang, Production mechanism of the neutron-rich nuclei in multinucleon transfer reactions: A reaction time scale analysis in energy dissipation process, Phys. Lett. B **809**, 135697 (2020).
[95] V. E. Viola, K. Kwiatkowski, and M. Walker, Systematics of fission fragment total kinetic energy release, Phys. Rev. C **31**, 1550 (1985).
[96] E. M. Kozulin, G. N. Knyazheva, I. M. Itkis, M. G. Itkis, A. A. Bogachev, E. V. Chernysheva, L. Krupa, F. Hanappe, O. Dorvaux, L. Stuttgé, W. H. Trzaska, C. Schmitt, and G. Chubarian, Fusion-fission and quasifission of superheavy systems with $Z = 110$–116 formed in $^{48}$Ca-induced reactions, Phys. Rev. C **90**, 054608 (2014).